

# Addressing the correlation of Stokes-shifted photons emitted from two quantum emitters

Adrián Juan-Delgado,<sup>1,2,\*</sup> Jean-Baptiste Trebbia,<sup>3,4</sup> Ruben Esteban,<sup>1,5</sup> Quentin Deplano,<sup>3,4</sup> Philippe Tamarat,<sup>3,4</sup> Rémi Avriller,<sup>6</sup> Brahim Lounis,<sup>3,4</sup> and Javier Aizpurua<sup>5,7,2,†</sup>

<sup>1</sup>*Centro de Física de Materiales (CMF-MPC), CSIC-UPV/EHU, 20018, Donostia-San Sebastián, Spain*

<sup>2</sup>*Department of Electricity and Electronics, University of the Basque Country (UPV/EHU), Leioa 48940, Spain*

<sup>3</sup>*Université de Bordeaux, LP2N, F-33405 Talence, France*

<sup>4</sup>*Institut d'Optique & CNRS, LP2N, F-33405 Talence, France*

<sup>5</sup>*Donostia International Physics Center (DIPC), 20018, Donostia-San Sebastián, Spain*

<sup>6</sup>*Université de Bordeaux, CNRS, LOMA, UMR 5798, F-33400 Talence, France*

<sup>7</sup>*Ikerbasque, Basque Foundation for Science, 48009 Bilbao, Spain.*

(Dated: February 3, 2025)

In resonance fluorescence excitation experiments, light emitted from solid-state quantum emitters is typically filtered to eliminate the laser photons, ensuring that only red-shifted Stokes photons are detected. Theoretical analyses of the fluorescence intensity correlation often model emitters as two-level systems, focusing on light emitted exclusively from the purely electronic transition (the Zero-Phonon Line), or rely on statistical approaches based on conditional probabilities that do not account for quantum coherences. Here, we propose a general model to characterize the correlation of either Zero-Phonon Line photons or Stokes-shifted photons. This model successfully reproduces the experimental correlation of Stokes-shifted photons emitted from two interacting molecules and predicts that this correlation is affected by quantum coherence. Besides, we analyze the role of quantum coherence in light emission from two uncorrelated emitters, which helps to clarify the discrepancy between theory and experiments regarding the value of the correlation of photons emitted from this system at zero delay time.

Theoretical descriptions of light emission from quantum emitters typically focus on the case of simple two-level systems (TLSs). This typical framework is useful to describe light emission from atoms. In the case of emitters that support vibrational modes (e.g., solid-state emitters, trapped ions and trapped atoms), this framework can be used to characterize the properties of photons emitted due to a decay from the pure (0-phonon) electronic excited state to the pure electronic ground state, which is known as Zero-Phonon Line (ZPL). In this way, multiple works (for example, see Refs. [1–12]) have analyzed light emission from two interacting quantum emitters, a system with potential applications in quantum technology, as in quantum-state engineering [13], two-qubit-gate implementation [14, 15] and quantum-information storage [16–18].

Moreover, in usual resonance fluorescence experiments, solid-state quantum emitters can relax from the pure electronic excited state via a radiative decay to the pure ground state (ZPL emission) or via a radiative decay to a 1-phonon electronic ground state (Stokes-shifted emission). To avoid the detection of laser photons that disturb the measurement of, for example, the intensity correlation  $g^{(2)}(\tau)$ , light is typically filtered and only red-shifted transitions are accounted for in the detection. Thus, photons emitted in the ZPL are discarded and only the Stokes-shifted photons are measured in these usual fluorescence experiments [19–22]. In these conditions, the typical framework that describes the emission of light in the ZPL is not suited to address state-of-the-art experiments of light emission from interacting solid-

state emitters [23–25]. To overcome this problem, the experimental correlation of Stokes-shifted photons emitted from two interacting emitters has been described using a statistical approach in Refs. [23, 24]. This statistical approach is based on the calculation of the conditional probabilities of a fluorescence photon being emitted by the system at time  $t + \tau$ , following an earlier emission at time  $t$  that projects the state of the system [26, 27]. These probabilities are calculated from the steady-state populations and their temporal evolution after the projection, obtained by solving the Master equation that governs the dynamics of the system. However, this approach does not account for the influence of quantum coherence in the emission and, thus, can fail to describe experiments where coherence becomes important, as we demonstrate here.

In this Letter, we present a general model to address the statistics of Stokes-shifted emission from quantum emitters supporting vibrational modes, as well as the statistics of ZPL emission. This model accounts for the influence of quantum coherence in the emission and enables the analysis of correlation of photons emitted from a large variety of quantum emitters under different detection schemes, as schematically depicted in Fig. 1a. We use this model to compare the statistics of ZPL photons and of Stokes-shifted photons emitted from two interacting organic molecules at cryogenic temperatures, revealing that these statistics can be very different from each other, and also to identify the role of quantum coherence in the emission of Stokes-shifted photons. These results are supported by experimental measurements. Fi-

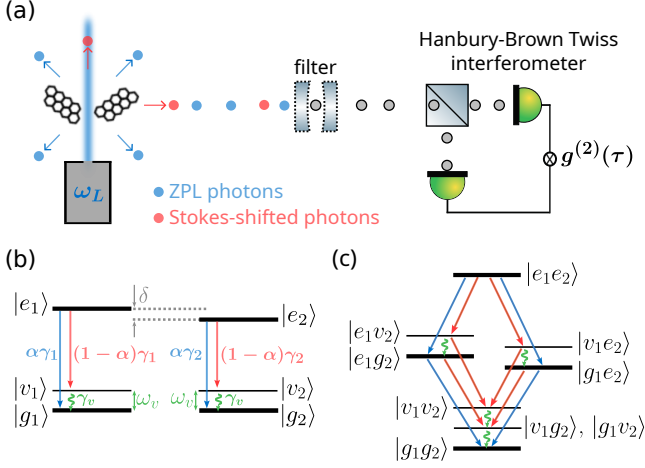


FIG. 1. (a) Schematic representation of light emitted from two interacting emitters, the filtering of this light and the measurement of the intensity correlation  $g^{(2)}(\tau)$ . A laser beam at frequency  $\omega_L$  (in blue) excites resonantly the pure electronic excited state of the quantum emitters, which then can emit a photon at the same frequency (blue circles) or a Stokes-shifted photon (red circles). A filter selects either the ZPL or Stokes-shifted light (grey circles represent these filtered photons). (b) Energy levels of the two emitters when they do not interact. See text for energy and dissipation labels. (c) Scheme of the different decay paths that can lead to the emission of ZPL photons (blue arrows) and of Stokes-shifted photons (red arrows).

nally, we explore the role of quantum coherence in Stokes-shifted emission from two distant emitters, which clarifies that the difficulty in measuring the theoretical limit of the correlation at delay  $\tau = 0$  in experiments with uncorrelated emitters is due to the insufficient time-resolution of the detectors.

We consider two quantum emitters (indexed by  $j = 1, 2$ ), with pure (0-phonon) electronic ground state  $|g_j\rangle$  and pure excited state  $|e_j\rangle$ . The transition dipole moment between these two states is denoted by  $\boldsymbol{\mu}_j$  and the transition frequency by  $\omega_j$ . The detuning between the two transition frequencies is  $\delta = \omega_1 - \omega_2$ . We consider an additional state  $|v_j\rangle$  that corresponds to the 1-phonon state of a vibrational mode of frequency  $\omega_v$  in the electronic ground state, see Fig. 1b. In the rotating frame at the laser frequency  $\omega_L$ , the unperturbed Hamiltonian of the system can be written as

$$\hat{H}_0 = \hbar \sum_{j=1}^2 \left[ \frac{\Delta_j}{2} (|e_j\rangle \langle e_j| - |g_j\rangle \langle g_j|) + \frac{2\omega_v - \Delta_j}{2} |v_j\rangle \langle v_j| \right], \quad (1)$$

with  $\Delta_j = \omega_j - \omega_L$ . Further, the coherent dipole-dipole interaction between the two emitters is described by  $\hat{H}_I = \hbar V (\hat{\sigma}_1^\dagger \hat{\sigma}_2 + \hat{\sigma}_1 \hat{\sigma}_2^\dagger)$ , with  $V$  the coupling strength [28],  $\hat{\sigma}_j = |g_j\rangle \langle e_j|$  and  $\hat{\sigma}_j^\dagger$  the ZPL lowering and rais-

ing operators of emitter  $j$ , respectively. We consider that  $V$  depends on the combined Debye-Waller/Franck-Condon factor  $\alpha$  to effectively account for the impact of the phonons of the host matrix and of the different internal vibrations of the emitters [12, 24] (see Supplemental Material [29]). The total Hamiltonian is thus  $\hat{H} = \hat{H}_0 + \hat{H}_I + \hat{H}_P$ , where  $\hat{H}_P = -\frac{\hbar}{2} \sum_{j=1}^2 (\Omega_j \hat{\sigma}_j^\dagger + \Omega_j^* \hat{\sigma}_j)$  is the pumping Hamiltonian. Here,  $\Omega_j = -\boldsymbol{\mu}_j \cdot \boldsymbol{\mathcal{E}}_j e^{-i\mathbf{k}_L \cdot \mathbf{r}_j} / \hbar$  is the Rabi frequency, with  $\mathbf{k}_L$  the laser wave-vector and  $\boldsymbol{\mathcal{E}}_j$  the laser electric field at the position  $\mathbf{r}_j$  of emitter  $j$ .

The state of the interacting emitters can be described by the density matrix  $\hat{\rho}$ , whose dynamics is governed by the Markovian Master Equation

$$\begin{aligned} \frac{d}{dt} \hat{\rho} = & -\frac{i}{\hbar} [\hat{H}, \hat{\rho}] + \sum_{j=1}^2 \left( \frac{\alpha \gamma_j}{2} \mathcal{D}[\hat{\sigma}_j] + \frac{(1-\alpha) \gamma_j}{2} \mathcal{D}[|v_j\rangle \langle e_j|] \right. \\ & \left. + \sum_{k \neq j} \frac{\gamma_{jk}}{2} \mathcal{D}[\hat{\sigma}_j, \hat{\sigma}_k] + \frac{\gamma_v}{2} \mathcal{D}[|g_j\rangle \langle v_j|] \right) \rho, \end{aligned} \quad (2)$$

where we have introduced the dissipators  $\mathcal{D}[\hat{A}, \hat{B}] \hat{\rho} = 2\hat{A} \hat{\rho} \hat{B}^\dagger - \hat{B}^\dagger \hat{A} \hat{\rho} - \hat{\rho} \hat{B}^\dagger \hat{A}$  and  $\mathcal{D}[\hat{A}] = \mathcal{D}[\hat{A}, \hat{A}]$  [30]. Here,  $\gamma_j$  is the total decay rate from the excited state  $|e_j\rangle$ . Additionally, as  $\alpha$  corresponds to the fraction of photons emitted in the ZPL line, we have fixed  $\alpha \gamma_j$  as the decay rate in the ZPL [first dissipator in Eq. (2)] and  $(1-\alpha) \gamma_j$  as the decay rate into the 1-phonon state [second dissipator].  $\gamma_{jk}$  is the crossed-decay rate including the effect of  $\alpha$  (see the Supplemental Material [29]). The last dissipator in Eq. (2) accounts for the non-radiative relaxation from the vibrational state  $|v_j\rangle$  to  $|g_j\rangle$ . Remarkably, we have checked that the intensity correlation is not notably modified if the total decay rate  $\gamma_j$  is entirely assigned to the ZPL dissipator [29].

To compute the intensity correlation we use the general expression [31, 32]

$$g^{(2)}(\tau) = \frac{\langle \hat{E}^{(-)}(0) \hat{E}^{(-)}(\tau) \hat{E}^{(+)}(\tau) \hat{E}^{(+)}(0) \rangle_{ss}}{\langle \hat{E}^{(-)}(0) \hat{E}^{(+)}(0) \rangle_{ss}^2}, \quad (3)$$

where  $\hat{E}^{(+)}(\tau)$  and  $\hat{E}^{(-)}(\tau)$  are the positive-frequency and negative-frequency electric field operators in the Heisenberg picture and  $\langle \hat{A} \rangle_{ss} = \text{Tr}(\hat{A} \hat{\rho}_{ss})$  is the expected value of  $\hat{A}$  at the steady-state  $\hat{\rho}_{ss}$ . The experimental filtering is introduced through the proper definition of the electric field operators. Assuming that the transition dipole moments of both emitters are identical ( $\boldsymbol{\mu}_1 = \boldsymbol{\mu}_2$ ), the correlation of ZPL photons can be calculated using  $\hat{E}_{\text{ZPL}}^{(+)}(t) / \xi_{\text{ZPL}} = \hat{\sigma}_1(t) + e^{i\phi_{\text{ZPL}}} \hat{\sigma}_2(t)$  (as in the typical framework where the emitters are treated as TLSs [29]), whereas the correlation of Stokes-shifted photons can be obtained through  $\hat{E}_{\text{St}}^{(+)}(t) / \xi_{\text{St}} = |v_1\rangle \langle e_1|(t) + e^{i\phi_{\text{St}}} |v_2\rangle \langle e_2|(t)$ . Here,  $\xi_{\text{ZPL}}$  and  $\xi_{\text{St}}$  are proportionality constants that do not affect the intensity

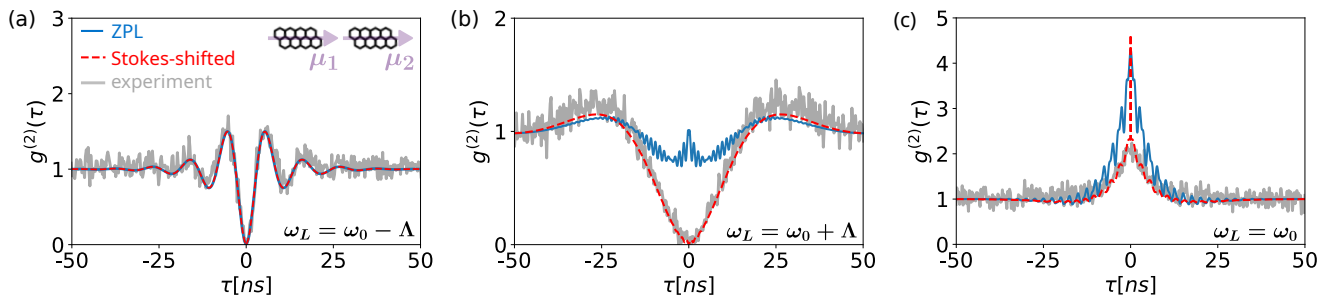


FIG. 2. Comparison of the correlation of ZPL photons and of Stokes-shifted photons emitted from two strongly interacting DBATT molecules. The molecules are in a J-aggregate configuration, as depicted in the inset in (a). The laser is tuned resonantly to the (a) superradiant state  $|\Lambda_{-}\rangle$  ( $\omega_L = \omega_0 - \Lambda$ ), (b) subradiant state  $|\Lambda_{+}\rangle$  ( $\omega_L = \omega_0 + \Lambda$ ) and (c) two-photon resonance ( $\omega_L = \omega_0$ ). The simulated intensity correlation  $g^{(2)}(\tau)$  of (solid blue line) ZPL and (dashed red line) Stokes-shifted light are plotted as a function of time delay  $\tau$ . Solid grey line corresponds to the experimental results reported in Ref. [24]. All the parameters are specified in the Supplemental Material [29].

correlation and are given by the direction of the dipoles, the direction of detection  $\hat{\mathbf{k}}_d$  and the mean frequency of emission [i.e.,  $\omega_0 = (\omega_1 + \omega_2)/2$  in the case of  $\xi_{\text{ZPL}}$  and  $\omega_0 - \omega_v$  in the case of  $\xi_{\text{St}}$ ] [1, 6, 8]. Additionally,  $\phi_{\text{ZPL}} = [\mathbf{k}_L - \hat{\mathbf{k}}_d n \omega_0 / c] \cdot \mathbf{r}_{12}$  and  $\phi_{\text{St}} = [\mathbf{k}_L - \hat{\mathbf{k}}_d n (\omega_0 - \omega_v) / c] \cdot \mathbf{r}_{12}$  [33, 34], with  $n$  the refractive index of the host medium and  $c$  the speed of light in vacuum.

We demonstrate next that the correlation of ZPL photons and of Stokes-shifted photons can be drastically different. With this purpose, we simulate the experimental configuration in Ref. [24], which measures the statistics of the Stokes-shifted photons emitted from two strongly interacting dibenzanthanthrene (DBATT) molecules (in a J-aggregate configuration [29]) in the normal direction to  $\boldsymbol{\mu}_j$  and  $\mathbf{r}_{12}$  (i.e.,  $\phi_{\text{ZPL}} = \phi_{\text{St}} = 0$ ). The mean frequency  $\omega_0$  of these molecules corresponds to a wavelength of 618 nm. Additionally, we consider the DBATT vibrational mode  $\hbar\omega_v = 31.86$  meV [35], and  $1/\gamma_v = 10$  ps based on experiments in Ref. [36]. The simulations are independent of  $\omega_v$  and  $\gamma_v$  at  $\tau \gg 1/\gamma_v$ . The rest of parameters are specified in the Supplemental Material [29].

We plot in Fig. 2a the intensity correlation  $g^{(2)}(\tau)$  when the laser is tuned resonantly to the superradiant state, which in the J-aggregate configuration corresponds to the hybrid state  $|\Lambda_{-}\rangle = -\sin\theta |g_1 e_2\rangle + \cos\theta |e_1 g_2\rangle$  [12], with transition frequency  $\omega_0 - \Lambda$ . Here,  $\tan(2\theta) = 2V/\delta$  and  $\Lambda = \sqrt{V^2 + (\delta/2)^2}$ . We find that the intensity correlation of Stokes-shifted photons (dashed red line) is almost identical to the correlation of ZPL photons (solid blue line), both exhibiting antibunching and Rabi oscillations due to the approximately TLS-like behaviour of the interacting system under this laser frequency and intensity [12]. The intensity correlation obtained experimentally in Ref. [24] (solid grey line) is well reproduced by the two simulations. On the other hand, Fig. 2b shows the intensity correlation when the laser is tuned resonantly to the subradiant state  $|\Lambda_{+}\rangle = \cos\theta |g_1 e_2\rangle +$

$\sin\theta |e_1 g_2\rangle$ , with transition frequency  $\omega_0 + \Lambda$ . The simulated correlation of ZPL photons and of Stokes-shifted photons show a very different behaviour. The correlation of ZPL photons shows  $g^{(2)}(0) \approx 1$  and oscillations with two different timescales (one of them are Rabi oscillations and the other one corresponds to much faster oscillations of frequency  $2\Lambda$  that are due to interference processes between the superradiant and the subradiant states [12]). In contrast, the correlation of Stokes-shifted photons exhibits antibunching, only Rabi oscillations and, crucially, an excellent agreement with the experimental measurements.

Further, we show in Fig. 2c the intensity correlation when the laser is tuned to the two-photon resonance ( $\omega_L = \omega_0$ ), corresponding to half the frequency between  $|g_1 g_2\rangle$  and  $|e_1 e_2\rangle$ . In this case, both the correlation of ZPL photons and of Stokes-shifted photons are bunched and exhibit oscillations of frequency  $\Lambda$  (corresponding to the detuning between the laser frequency and the transition frequency of the superradiant state). However, the ZPL correlation exhibits more pronounced oscillations and does not capture well the experimental measurements, whereas the Stokes-shifted correlation reproduces them very well. These results reveal that the correlation of Stokes-shifted photons and of ZPL photons emitted from two strongly interacting quantum emitters can be very different and emphasize the importance of an accurate description of each experimental configuration.

Next, we analyze the role of quantum coherence in the correlation of Stokes-shifted photons emitted from two quantum emitters. To this aim, we substitute  $\hat{E}_{\text{St}}^{(+)}(t)/\xi_{\text{St}} = |v_1\rangle \langle e_1|(t) + |v_2\rangle \langle e_2|(t)$  (where  $\phi_{\text{St}} = 0$ ) into the general expression of the intensity correlation in Eq. (3). After some algebra (see Supplemental Material

[29]), we obtain

$$g_{\text{St}}^{(2)}(\tau) = \frac{G_d^{(2)}(\tau) + G_{\text{coh},I}^{(2)}(\tau) + G_{\text{coh},\rho}^{(2)}(\tau)}{\langle \hat{I}_{\text{St}}(0) \rangle_{ss}^2}. \quad (4)$$

We first consider the denominator, where we have introduced the operator  $\hat{I}_{\text{St}}(\tau) = \hat{E}_{\text{St}}^{(-)}(\tau)\hat{E}_{\text{St}}^{(+)}(\tau)$  (which is proportional to the fluorescence intensity), with steady-state expected value

$$\frac{\langle \hat{I}_{\text{St}}(0) \rangle_{ss}}{|\xi_{\text{St}}|^2} = 2p_{ee} + p_{eg} + p_{ge} + p_{ev} + p_{ve} + 2\text{Re}\rho_{ev,ve}. \quad (5)$$

Here,  $p_{ab} = \langle a_1 b_2 | \hat{\rho}_{ss} | a_1 b_2 \rangle$  is the population of the state  $|a_1 b_2\rangle$  of the uncoupled basis (with  $a_j, b_j \in \{e_j, g_j, v_j\}$ ) and  $\rho_{ev,ve} = \langle e_1 v_2 | \hat{\rho}_{ss} | v_1 e_2 \rangle$  an off-diagonal element of the density matrix (coherence) in the same basis. We have numerically verified that  $\rho_{ev,ve}$  is negligible.

Further, we have decomposed the numerator in Eq. (4) into three different terms. The first term involves only diagonal elements of  $\hat{\rho}_{ss}$  and  $\hat{I}_{\text{St}}(\tau)$ , and it is given as

$$\begin{aligned} \frac{G_d^{(2)}(\tau)}{|\xi_{\text{St}}|^4} &= p_{ee} \langle v_1 e_2 | \hat{I}_{\text{St}}(\tau) | v_1 e_2 \rangle + \langle e_1 v_2 | \hat{I}_{\text{St}}(\tau) | e_1 v_2 \rangle \\ &+ p_{ev} \langle v_1 v_2 | \hat{I}_{\text{St}}(\tau) | v_1 v_2 \rangle + p_{ve} \langle v_1 v_2 | \hat{I}_{\text{St}}(\tau) | v_1 v_2 \rangle \\ &+ p_{eg} \langle v_1 g_2 | \hat{I}_{\text{St}}(\tau) | v_1 g_2 \rangle + p_{ge} \langle g_1 v_2 | \hat{I}_{\text{St}}(\tau) | g_1 v_2 \rangle. \end{aligned} \quad (6)$$

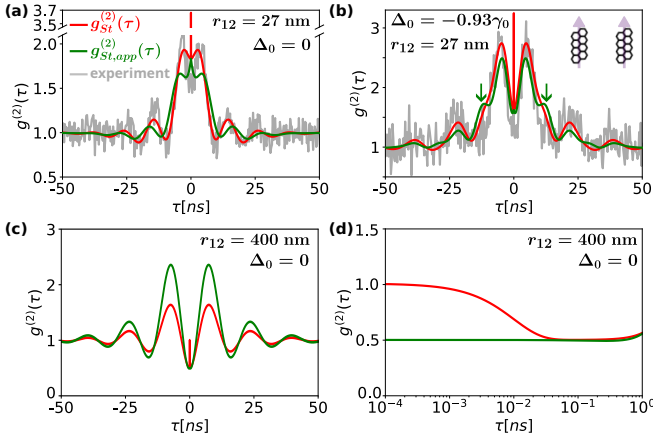


FIG. 3. Impact of quantum coherence in the correlation of Stokes-shifted photons emitted from two DBATT molecules. The molecules are in a H-aggregate configuration, as depicted in the inset in (b). We consider  $r_{12} = 27$  nm in (a, b) and  $r_{12} = 400$  nm in (c, d). The laser is tuned to the two-photon resonance  $\Delta_0 = 0$  in all panels (with  $\Delta_0 = \omega_0 - \omega_L$ ), except in (b) where  $\Delta_0 = -0.93\gamma_0$ . Red lines correspond to the simulation using the full model including quantum coherence in the emission, whereas green lines to the simulation neglecting this coherence. Grey lines in (a,b) correspond to experimental measurements. The rest of parameters are specified in the Supplemental Material [29].

The six different terms on the right-hand side of the above expression are related to the six different decay paths leading to the emission of Stokes-shifted photons (red arrows in Fig. 1c). Thus, the contribution of  $G_d^{(2)}(\tau)$  to the intensity correlation is equivalent to that obtained with the statistical approach based on conditional probabilities [23, 24, 26, 27]. In contrast,

$$\frac{G_{\text{coh},I}^{(2)}(\tau)}{|\xi_{\text{St}}|^4} = p_{ee} \langle v_1 e_2 | \hat{I}_{\text{St}}(\tau) | e_1 v_2 \rangle + \langle e_1 v_2 | \hat{I}_{\text{St}}(\tau) | v_1 e_2 \rangle \quad (7)$$

is proportional to the population  $p_{ee}$  and to the coherence between the states  $|e_1 v_2\rangle$  and  $|v_1 e_2\rangle$  in the operator  $\hat{I}_{\text{St}}(\tau)$ .  $G_{\text{coh},I}^{(2)}(\tau)$  can be interpreted as the quantum interference between the emission paths of the two molecules (i.e., the Hanbury-Brown Twiss effect [37–39]). Last,  $G_{\text{coh},\rho}^{(2)}(\tau)$  includes all terms involving off-diagonal elements of the density matrix [29].

We first analyze the role of quantum coherence in the case of two DBATT molecules separated by a short distance ( $r_{12} = 27$  nm). To this aim, we compare new experimental measurements of the correlation of Stokes-shifted photons emitted from a molecular H-aggregate configuration (experimental setup in the Supplemental Material [29]) with the simulated intensity correlations obtained with the complete model [given by Eq. (4)], as well as with the correlation

$$g_{\text{St,app}}^{(2)}(\tau) = \frac{G_d^{(2)}(\tau)}{|\xi_{\text{St}}|^4 (2p_{ee} + p_{eg} + p_{ge} + p_{ev} + p_{ve})^2} \quad (8)$$

obtained by neglecting the role of quantum coherence in the emission. In particular, we plot in Figs. 3a and 3b the correlation of Stokes-shifted photons for this molecular pair when the laser is tuned to  $\omega_L = \omega_0$  (resonantly to the two-photon resonance) and to  $\omega_L = \omega_0 + 0.93\gamma_0$  (slightly detuned from the two-photon resonance), respectively. The rest of parameters are specified in the Supplemental Material [29]. The simulations obtained with the complete expression (red lines) show a very good agreement with the experimental measurements (grey lines) and substantial differences with the simulations obtained by removing the effect of coherence (green line). More specifically, if coherences are neglected in the emission, we observe that (i) the amplitude of the oscillations is notably modified, and (ii) a bump emerges at  $\tau \approx \pm 10$  ns in Fig. 3b (see the green arrows), which is clearly not measured in experiments. These two differences are due to  $G_{\text{coh},\rho}^{(2)}(\tau)$ . Furthermore, we obtain an extremely narrow peak at  $\tau = 0$  in the complete simulation.  $G_{\text{coh},I}^{(2)}(\tau)$  is responsible of this peak because at  $\tau = 0$  this term becomes identical to  $G_d^{(2)}(0)$  (see Supplemental Material [29]), but  $G_{\text{coh},I}^{(2)}(\tau)$  decays to 0 in the timescale of the vibrational lifetime, as discussed below. In the Supplemental Material [29], we provide additional measurements of



$g_{\text{St}}^{(2)}(\tau)$  from different molecular pairs, which also provide a good agreement with the simulations obtained with the complete model.

Finally, we analyze the correlation of Stokes-shifted photons emitted from two distant emitters and find that quantum coherence again plays an important role. Theoretical descriptions of light emission from  $N$  uncorrelated emitters resonantly driven with the same strength yield  $g^{(2)}(\tau = 0) = 2(1 - 1/N)$  [40–42], which tends to  $g^{(2)}(\tau = 0) \rightarrow 2$  for a large number  $N$ .  $g^{(2)}(\tau = 0) = 1$  is expected in the particular case of  $N = 2$  uncorrelated emitters but, as far as we know, available experiments up to date have reported  $g^{(2)}(\tau = 0) \approx 0.5$  independently of the particular implementation of the two-level quantum emitters [43–46]. To shed light into this discrepancy, we consider  $r_{12} = 400$  nm (which yields a negligible dipole-dipole coupling) and  $\omega_L = \omega_0$  (the rest of parameters are specified in the Supplemental Material [29]). We plot in Figs. 3c and 3d the simulations obtained with the complete model (red lines) and with the approximated expression that neglects the effect of coherence in the emission (green lines). The complete model yields  $g^{(2)}(\tau = 0) = 1$ , with a fast decay to 0.5 in the time scale of the vibrational lifetime (tens of picoseconds). This fast decay is due to the loss of the initial coherence encoded in  $G_{\text{coh},I}^{(2)}(\tau)$  and related to the constructive interference between the emission paths of the two molecules (Hanbury-Brown Twiss effect). We attribute this loss of coherence to the influence of the internal vibrations of the emitters acting as dephasing channel. Therefore, one can conclude that available experiments with uncorrelated emitters do not agree with theory at  $\tau = 0$  due to an insufficient time resolution of the detectors.

In summary, we have presented a general model to address the correlation of Stokes-shifted photons emitted from quantum emitters, as well as that of the ZPL photons. We have shown an excellent agreement between the simulations obtained using this model and experimental measurements of the correlation of the Stokes-shifted photons emitted from two interacting DBATT molecules (using experimental data from Ref. [24], as well as new experimental measurements). Additionally, we have revealed that the intensity correlation of ZPL photons can exhibit significant differences with respect to the intensity correlation of Stokes-shifted photons depending on the molecular and laser parameters. Furthermore, we have demonstrated that quantum coherence can impact the emission of Stokes-shifted photons when the emitters are interacting and also when they do not interact. Finally, we have found that detectors with time resolution smaller than the lifetime of the vibrations are needed to measure  $g^{(2)}(\tau = 0) = 1$  in experiments on light emission from two resonantly driven uncorrelated emitters.

*Acknowledgements.*— We thank Alejandro Gonzalez-Tudela, Álvaro Nodar and Jorge Olmos-Trigo for insightful discussions. A.J.D., R.E., and J.A. acknowledge fi-

ancial support through the grant PID2022-139579NB-I00 funded by MICIU/AEI/10.13039/501100011033 and by ERDF/EU, through the grant IT 1526-22 funded by the Department of Education, Research and Universities of the Basque Government and also through the CSIC Research Platform PTI-001 (project 20219PT023). A.J.D. acknowledges financial support through the grant PRE2020-095013 funded by MICIU/AEI/10.13039/501100011033 and by “ESF Investing in your future”. J.-B.T., Q.D., P.T. and B.L. acknowledge the financial support from the French National Agency for Research (ANR-22-CE47-0015), Région Nouvelle-Aquitaine, Idex Bordeaux (Research Program GPR Light), and the EUR Light S&T (PIA3 Program, ANR-17-EURE-0027). R.A. acknowledges financial support by EUR Light S&T Graduate Program (PIA3 Program “Investment for the Future,” ANR-17-EURE-0027), IdEx of the University of Bordeaux / Grand Research Program GPR LIGHT, and Quantum Matter Bordeaux. We acknowledge the Laboratory for Transborder Cooperation LTC TRANS-LIGHT from University of Bordeaux and Univ. of the Basque Country.

---

\* [adrianjuand1996@gmail.com](mailto:adrianjuand1996@gmail.com)

† [aizpurua@ehu.eus](mailto:aizpurua@ehu.eus)

- [1] R. Lehmberg, *Physical Review A* **2**, 883 (1970).
- [2] G. S. Agarwal, “Quantum statistical theories of spontaneous emission and their relation to other approaches,” in *Quantum Optics*, edited by G. Höhler (Springer Berlin Heidelberg, Berlin, Heidelberg, 1974) pp. 1–128.
- [3] G. Agarwal, A. Brown, L. Narducci, and G. Vetri, *Physical Review A* **15**, 1613 (1977).
- [4] R. Griffin and S. Harris, *Physical Review A* **25**, 1528 (1982).
- [5] Z. Ficek, R. Tanas, and S. Kielich, *Optica acta* **30**, 713 (1983).
- [6] Z. Ficek, R. Tanaś, and S. Kielich, *Physical Review A* **29**, 2004 (1984).
- [7] S. Lawande, B. Jagatap, and Q. Lawande, *Optics communications* **73**, 126 (1989).
- [8] T. Rudolph, Z. Ficek, and B. Dalton, *Physical Review A* **52**, 636 (1995).
- [9] J. Gillet, G. Agarwal, and T. Bastin, *Physical Review A—Atomic, Molecular, and Optical Physics* **81**, 013837 (2010).
- [10] A. Vivas-Viaña and C. Sánchez Muñoz, *Physical Review Research* **3**, 033136 (2021).
- [11] C. Downing, E. del Valle, and A. Fernández-Domínguez, *Physical Review A* **107**, 023717 (2023).
- [12] A. Juan-Delgado, R. Esteban, Á. Nodar, J.-B. Trebbia, B. Lounis, and J. Aizpurua, *Physical Review Research* **6**, 023207 (2024).
- [13] S. Lloyd, *Science* **261**, 1569 (1993).
- [14] V. Schäfer, C. Ballance, K. Thirumalai, L. Stephenson, T. Ballance, A. Steane, and D. Lucas, *Nature* **555**, 75 (2018).

- [15] J. Reina, C. Susa, and R. Hildner, *Physical Review A* **97**, 063422 (2018).
- [16] D. Plankensteiner, L. Ostermann, H. Ritsch, and C. Genes, *Scientific reports* **5**, 16231 (2015).
- [17] G. Facchinetti, S. Jenkins, and J. Ruostekoski, *Physical review letters* **117**, 243601 (2016).
- [18] A. Asenjo-Garcia, M. Moreno-Cardoner, A. Albrecht, H. Kimble, and D. Chang, *Physical Review X* **7**, 031024 (2017).
- [19] P. Tamarat, A. Maali, B. Lounis, and M. Orrit, *The Journal of Physical Chemistry A* **104**, 1 (1999).
- [20] W. Moerner, “A dozen years of single-molecule spectroscopy in physics, chemistry, and biophysics,” (2002).
- [21] M. Orrit and J. Bernard, *Physical review letters* **65**, 2716 (1990).
- [22] W. Ambrose and W. Moerner, *Nature* **349**, 225 (1991).
- [23] C. Hettich, C. Schmitt, J. Zitzmann, S. Kuhn, I. Gerhardt, and V. Sandoghdar, *Science* **298**, 385 (2002).
- [24] J. Trebbia, Q. Deplano, P. Tamarat, and B. Lounis, *Nature Communications* **13**, 1 (2022).
- [25] C. Lange, E. Daggett, V. Walther, L. Huang, and J. Hood, *Nature Physics* **20**, 836–842 (2024).
- [26] A. Beige and G. Hegerfeldt, *Physical Review A* **58**, 4133 (1998).
- [27] C. Hettich, *Coherent Optical Dipole Coupling of Two Individual Molecules at Nanometre Separation*, Ph.D. thesis, Universität Konstanz, Konstanz (2002).
- [28] A. Stokes and A. Nazir, *New Journal of Physics* **20**, 043022 (2018).
- [29] See Supplemental Material, which contains Refs. [12, 24, 28, 35], for the complete expressions of the coherent and incoherent dipole-dipole couplings, the details of all the parameters used in the simulations, a summary of the typical framework with two-level systems, the complete expression of the correlation of Stokes-shifted photons, an alternative Master Equation to compute the correlation of Stokes-shifted photons, details of the experimental setup, further experimental measurements, and an analysis of the impact of a larger number of vibrational modes.
- [30] H.-P. Breuer and F. Petruccione, *The theory of open quantum systems* (Oxford University Press on Demand, 2002).
- [31] L. Mandel and E. Wolf, *Optical coherence and quantum optics* (Cambridge university press, 1995).
- [32] C. Gerry, P. Knight, and P. Knight, *Introductory quantum optics* (Cambridge university press, 2005).
- [33] C. Skornia, J. von Zanthier, G. Agarwal, E. Werner, and H. Walther, *Physical Review A* **64**, 063801 (2001).
- [34] S. Wolf, S. Richter, J. von Zanthier, and F. Schmidt-Kaler, *Physical Review Letters* **124**, 063603 (2020).
- [35] F. Jelezko, B. Lounis, and M. Orrit, *The Journal of chemical physics* **107**, 1692 (1997).
- [36] J. Zirkelbach, M. Mirzaei, I. Deperasińska, B. Kozankiewicz, B. Gurlek, A. Shkarin, T. Utikal, S. Götzinger, and V. Sandoghdar, *The Journal of Chemical Physics* **156** (2022).
- [37] R. Hanbury-Brown and R. Twiss, *Nature* **178**, 1046 (1956).
- [38] U. Fano, *American Journal of Physics* **29**, 539 (1961).
- [39] A. Aspect, in *Current Trends in Atomic Physics* (Oxford University Press, 2019).
- [40] A. Auffèves, D. Gerace, S. Portolan, A. Drezet, and M. Santos, *New Journal of Physics* **13**, 093020 (2011).
- [41] D. Meiser and M. Holland, *Physical Review A* **81**, 063827 (2010).
- [42] R. Jones, R. Saint, and B. Olmos, *Journal of Physics B: atomic, molecular and optical physics* **50**, 014004 (2016).
- [43] F. Diedrich and H. Walther, *Physical review letters* **58**, 203 (1987).
- [44] W. Itano, J. Bergquist, and D. Wineland, *Physical Review A* **38**, 559 (1988).
- [45] V. Gomer, F. Strauch, B. Ueberholz, S. Knappe, and D. Meschede, *Physical Review A* **58**, R1657 (1998).
- [46] S. Pezzagna, B. Naydenov, F. Jelezko, J. Wrachtrup, and J. Meijer, *New Journal of Physics* **12**, 065017 (2010).

# Supplemental Material: Addressing the correlation of Stokes-shifted photons emitted from two quantum emitters

Adrián Juan-Delgado,<sup>1,2,\*</sup> Jean-Baptiste Trebbia,<sup>3,4</sup> Ruben Esteban,<sup>1,5</sup> Quentin Deplano,<sup>3,4</sup>

Philippe Tamarat,<sup>3,4</sup> Rémi Avriller,<sup>6</sup> Brahim Lounis,<sup>3,4</sup> and Javier Aizpurua<sup>5,7,2,†</sup>

<sup>1</sup>*Centro de Física de Materiales (CMF-MPC), CSIC-UPV/EHU, 20018, Donostia-San Sebastián, Spain*

<sup>2</sup>*Department of Electricity and Electronics, University of the Basque Country (UPV/EHU), Leioa 48940, Spain*

<sup>3</sup>*Université de Bordeaux, LP2N, F-33405 Talence, France*

<sup>4</sup>*Institut d'Optique & CNRS, LP2N, F-33405 Talence, France*

<sup>5</sup>*Donostia International Physics Center (DIPC), 20018, Donostia-San Sebastián, Spain*

<sup>6</sup>*Université de Bordeaux, CNRS, LOMA, UMR 5798, F-33400 Talence, France*

<sup>7</sup>*Ikerbasque, Basque Foundation for Science, 48009 Bilbao, Spain.*

(Dated: February 3, 2025)

## CONTENTS

I. Expressions of the coherent and incoherent dipole-dipole couplings	1
II. Parameters used in simulations	2
III. Typical framework with two-level systems	3
IV. Analytical expression of the correlation of Stokes-shifted photons	3
V. Alternative Master equation	5
VI. Experimental setup	6
VII. Further experimental measurements	7
VIII. Impact of a larger number of vibrational modes	8
References	9

## I. EXPRESSIONS OF THE COHERENT AND INCOHERENT DIPOLE-DIPOLE COUPLINGS

In this section we provide the expressions of the coherent dipole-dipole coupling  $V$  and the dissipative dipole-dipole coupling  $\gamma_{12}$ . These expressions are given by

$$V = \frac{3}{4}\alpha\gamma_0 \left[ -\left(\hat{\boldsymbol{\mu}}_1 \cdot \hat{\boldsymbol{\mu}}_2 - (\hat{\boldsymbol{\mu}}_1 \cdot \hat{\mathbf{r}}_{12})(\hat{\boldsymbol{\mu}}_2 \cdot \hat{\mathbf{r}}_{12})\right) \frac{\cos(kr_{12})}{kr_{12}} + \left(\hat{\boldsymbol{\mu}}_1 \cdot \hat{\boldsymbol{\mu}}_2 - 3(\hat{\boldsymbol{\mu}}_1 \cdot \hat{\mathbf{r}}_{12})(\hat{\boldsymbol{\mu}}_2 \cdot \hat{\mathbf{r}}_{12})\right) \left( \frac{\sin(kr_{12})}{(kr_{12})^2} + \frac{\cos(kr_{12})}{(kr_{12})^3} \right) \right], \quad (\text{S1a})$$

$$\gamma_{12} = \frac{3}{2}\alpha\gamma_0 \left[ \left(\hat{\boldsymbol{\mu}}_1 \cdot \hat{\boldsymbol{\mu}}_2 - (\hat{\boldsymbol{\mu}}_1 \cdot \hat{\mathbf{r}}_{12})(\hat{\boldsymbol{\mu}}_2 \cdot \hat{\mathbf{r}}_{12})\right) \frac{\sin(kr_{12})}{kr_{12}} + \left(\hat{\boldsymbol{\mu}}_1 \cdot \hat{\boldsymbol{\mu}}_2 - 3(\hat{\boldsymbol{\mu}}_1 \cdot \hat{\mathbf{r}}_{12})(\hat{\boldsymbol{\mu}}_2 \cdot \hat{\mathbf{r}}_{12})\right) \left( \frac{\cos(kr_{12})}{(kr_{12})^2} - \frac{\sin(kr_{12})}{(kr_{12})^3} \right) \right], \quad (\text{S1b})$$

where  $\alpha$  is the combined Debye-Waller/Franck-Condon factor,  $\gamma_0$  is the total decay rate from the electronic excited state  $|e_j\rangle$ ,  $\hat{\mathbf{r}}_{12} = (\mathbf{r}_2 - \mathbf{r}_1)/r_{12}$  is the unit vector pointing from the position  $\mathbf{r}_1$  of emitter  $j = 1$  to the position  $\mathbf{r}_2$  of emitter  $j = 2$ ,  $r_{12} = |\mathbf{r}_2 - \mathbf{r}_1|$  is the distance between the emitters, and  $k = n \frac{\omega_1 + \omega_2}{2c}$  is the wavenumber of the arithmetic mean of the transition frequency of the two emitters, with  $c$  the speed of light in vacuum and  $n$  the refractive index of the host matrix. Additionally,  $\hat{\boldsymbol{\mu}}_j = \boldsymbol{\mu}_j/|\boldsymbol{\mu}_j|$  is the unit vector of the transition dipole moment of emitter  $j$  (corresponding to the transition between the pure electronic excited state  $|e_j\rangle$  and the pure electronic ground state  $|g_j\rangle$ ). The norm of  $\boldsymbol{\mu}_j$  is  $|\boldsymbol{\mu}_j| = \sqrt{\alpha\gamma_0 3\pi\epsilon_0 \hbar n^2 / k^3}$ , with  $\epsilon_0$  the vacuum permittivity. The expressions in Eq. (S1) include retardation effects [1], as well as the combined Debye-Waller/Franck-Condon factor  $\alpha$  [2, 3]. The

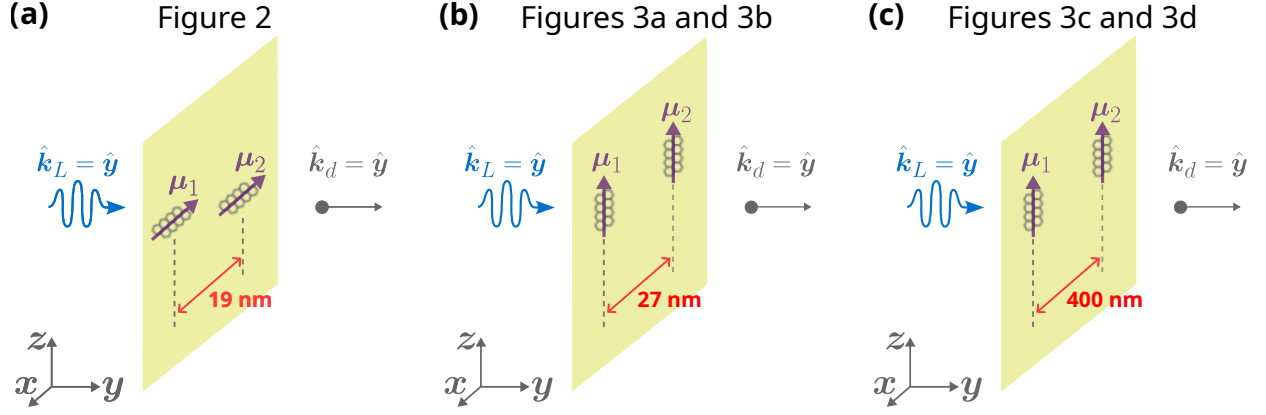


FIG. S1. Schematic representations of the molecular pairs used in the simulations of the intensity correlation presented in the main text. (a) J-aggregate molecular configuration simulated in Fig. 2 of the main text, where the transition dipole moments  $\mu_j$  are oriented in the  $x$ -direction and the molecules are separated by 19 nm in the  $x$ -direction and by 5.7 nm in the  $z$ -direction. (b) Molecular pair simulated in Figs. 3a and 3b of the main text, with the transition dipole moments oriented along the  $z$ -direction and forming a molecular H-aggregate with intermolecular distance of 27 nm in the  $x$ -direction. (c) Molecular pair with large separation distance in the  $x$ -direction (400 nm) and in a H-aggregate configuration (with the transition dipole moments aligned along the  $z$ -direction), which is used in the simulations in Figs. 3c and 3d of the main text. In all panels, we consider incidence and detection of light in the normal direction to the  $xz$ -plane where the transition dipole moments are contained.

latter corresponds to the proportion of photons emitted into the Zero-Phonon Line (ZPL) over the total number of photons emitted from the quantum emitter. Thus, this factor accounts in an effective manner for the phonons of the host matrix in which the emitters are immersed, as well as for the internal vibrational modes of the quantum emitters that are not taken explicitly into account.

## II. PARAMETERS USED IN SIMULATIONS

In this section we provide all the parameters of the different molecular configurations simulated in the main text (see Table S1), as well as schematic representations of each of these configurations. In all cases we fix  $\gamma_0/(2\pi) = 21.5$  MHz,  $\alpha = 0.3$ ,  $n = 1.5$ , and  $\omega_0 = (\omega_1 + \omega_2)/2$  corresponding to a wavelength of 618 nm. Additionally, we consider normal incidence and detection of light with respect to the  $xz$ -plane where the transition dipole moments  $\mu_j$  are contained, as sketched in Fig. S1. The molecules are excited by the component of the incident electric field that is parallel to the direction of the transition dipole moments. In Fig. S1a we plot the molecular configuration corresponding to the simulations in Fig. 2 of the main text, where the transition dipole moments are oriented along the  $x$ -direction and we fix  $\mathbf{r}_{12} = (19\hat{x} + 5.7\hat{z})$  nm (thus, mostly resembling a J-aggregate configuration, which is characterized by transition dipole moments aligned in the same direction than  $\mathbf{r}_{12}$ ), which yields  $V = -17\gamma_0$  and  $\gamma_{12} = 0.3\gamma_0$ . Next, Fig. S1b shows a schematic of the molecular pair simulated in Figs. 3a and 3b of the main text, with the transition dipole moments oriented along the  $z$ -direction and  $\mathbf{r}_{12} = 27\hat{x}$  nm (H-aggregate configuration, with transition dipole moments aligned in the direction perpendicular to  $\mathbf{r}_{12}$ ), leading to  $V = 2.98\gamma_0$  and  $\gamma_{12} = 0.29\gamma_0$ . Last, we represent in Fig. S1c the molecular pair simulated in Figs. 3c and 3d of the main text, where the molecules are considered to be separated by 400 nm and in a H-aggregate configuration, which results in  $V = -0.04\gamma_0$  and  $\gamma_{12} = -10^{-3}\gamma_0$ .

Figure	$\mu_j/ \mu_j $	$\mathbf{r}_1$	$\mathbf{r}_2$ [nm]	$\gamma_0/(2\pi)$ [MHz]	$\alpha$	$V/\gamma_0$	$\gamma_{ij}/\gamma_0$	$\delta/\gamma_0$	$ \Omega_j /\gamma_0$	$\mathbf{k}_L/ \mathbf{k}_L $	$\phi_{\text{ZPL,St}}$	$\hbar\omega_v$ [meV]	$1/\gamma_v$ [ps]
Fig. 2	$\hat{x}$	0	$19\hat{x} + 5.7\hat{z}$	21.5	0.3	-17	0.3	14	3.15	$\hat{y}$	0	31.86	10
Fig. 3a,b	$\hat{z}$	0	$27\hat{x}$	21.5	0.3	2.98	0.29	5	1.5	$\hat{y}$	0	31.86	10
Fig. 3c,d	$\hat{z}$	0	$400\hat{x}$	21.5	0.3	-0.04	$-10^{-3}$	5	1.5	$\hat{y}$	0	31.86	10

TABLE S1. Molecular and laser parameters used in the simulations in Fig. 2 (second row), in Figs. 3a and 3b (third row) and in Figs. 3c and 3d (fourth row) in the main text.



### III. TYPICAL FRAMEWORK WITH TWO-LEVEL SYSTEMS

In this section we review the typical framework describing the emitters as two-level systems (TLSs) and we show that it results in almost identical intensity correlation of ZPL photons as the model that we propose in the main text. However, we emphasize that the TLS framework introduced here cannot address the correlation of Stokes-shifted photons, in contrast to the model that we have presented in the main text including the vibrational levels and which allows for addressing the correlation of Stokes-shifted photons and also of ZPL photons.

Within the TLS framework, the Hamiltonian can be written as

$$\hat{H} = \hbar \sum_{j=1}^2 \left[ \frac{\Delta_j}{2} (|e_j\rangle \langle e_j| - |g_j\rangle \langle g_j|) \right] + \hat{H}_I + \hat{H}_P, \quad (\text{S2})$$

where the interaction Hamiltonian is  $\hat{H}_I = \hbar V (\hat{\sigma}_1^\dagger \hat{\sigma}_2 + \hat{\sigma}_1 \hat{\sigma}_2^\dagger)$  and the pumping Hamiltonian is  $\hat{H}_P = -\frac{\hbar}{2} \sum_{j=1}^2 (\Omega_j \hat{\sigma}_j^\dagger + \Omega_j^* \hat{\sigma}_j)$ . Here, we use the tilde symbol in the Hamiltonian  $\hat{H}$  to distinguish this description from the model including vibrations that we use in the main text. In this case, the Markovian Master Equation governing the dynamics of the density matrix  $\hat{\rho}$  takes the form

$$\frac{d}{dt} \hat{\rho} = -\frac{i}{\hbar} [\hat{H}, \hat{\rho}] + \sum_{j=1}^2 \left( \frac{\gamma_j}{2} \mathcal{D}[\hat{\sigma}_j] + \sum_{k \neq j} \frac{\gamma_{jk}}{2} \mathcal{D}[\hat{\sigma}_j, \hat{\sigma}_k] \right) \hat{\rho}. \quad (\text{S3})$$

The correlation of ZPL photons can be obtained using the same electric field operator  $\hat{E}_{ZPL}^{(+)}(t)(\tau)/\xi_{ZPL} = \sigma_1(t) + e^{i\phi_{ZPL}} \sigma_2(t)$  that we have used within the model presented in the main text. We have verified that the maximum difference between the correlation of ZPL photons obtained with the model in the main text and the TLS framework presented in this appendix is  $|\hat{g}_{ZPL}^{(2)}(\tau) - g_{ZPL}^{(2)}(\tau)|/g_{ZPL}^{(2)}(\tau) \approx 7 \cdot 10^{-4}$ . This difference occurs in the configuration in Fig. 2c of the main text and at delay  $\tau = 0$ .

### IV. ANALYTICAL EXPRESSION OF THE CORRELATION OF STOKES-SHIFTED PHOTONS

We detail in this section the derivation of the analytical expression of the intensity correlation of Stokes-shifted photons presented in Eq. (4) of the main text. First, we substitute the electric field operator  $\hat{E}_{St}^{(+)}(t)/\xi_{St} = |v_1\rangle \langle e_1| (t) + |v_2\rangle \langle e_2| (t)$  in the general expression of the intensity (or second-order) correlation in Eq. (2), which yields

$$g_{St}^{(2)}(\tau) = \frac{G_{St}^{(2)}(\tau)}{\langle \hat{I}_{St}(0) \rangle^2} = \frac{|\xi_{St}|^2 \langle (|e_1\rangle \langle v_1| + |e_2\rangle \langle v_2|) I_{St}(\tau) (|v_1\rangle \langle e_1| + |v_2\rangle \langle e_2|) \rangle}{\langle \hat{I}_{St}(0) \rangle^2}. \quad (\text{S4})$$

Here, we have introduced the operator

$$\hat{I}_{St}(t) = \hat{E}_{St}^{(-)}(t) \hat{E}_{St}^{(+)}(t) = |\xi_{St}|^2 \left( |e_1\rangle \langle v_1| (t) + |e_2\rangle \langle v_2| (t) \right) \left( |v_1\rangle \langle e_1| (t) + |v_2\rangle \langle e_2| (t) \right), \quad (\text{S5})$$

whose steady-state expected value  $\langle \hat{I}_{St}(0) \rangle$  is proportional to light intensity and is given by

$$\langle \hat{I}_{St}(0) \rangle = |\xi_{St}|^2 \left( 2p_{ee} + p_{eg} + p_{ge} + p_{ev} + p_{ve} + 2\text{Re}\rho_{ev,ve} \right). \quad (\text{S6})$$

where  $p_{ab} = \langle a_1 b_2 | \hat{\rho}_{ss} | a_1 b_2 \rangle$  is the population of the state  $|a_1 b_2\rangle$  and  $\rho_{ab,cd} = \langle a_1 b_2 | \hat{\rho}_{ss} | c_1 d_2 \rangle$  (with  $a, b, c, d \in \{e, g, v\}$ ) is an off-diagonal element of the steady-state density matrix.

Next, recalling that the steady-state value of any operator  $\hat{A}$  is given by  $\langle \hat{A} \rangle_{ss} = \text{Tr}(\hat{A} \hat{\rho}_{ss})$  and using the cyclic

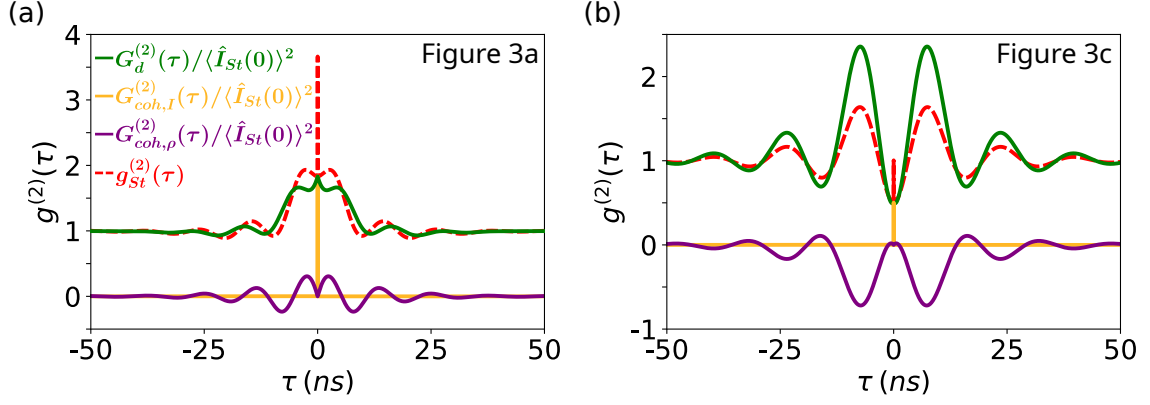


FIG. S2. Dependence on the time delay  $\tau$  of the different terms in which  $G_{St}^{(2)}(\tau)$  is decomposed in Eq. (S8). Solid green lines correspond to  $G_d^{(2)}(\tau)/\langle\hat{I}_{St}(0)\rangle^2$ , solid orange lines to  $G_{coh,I}^{(2)}(\tau)/\langle\hat{I}_{St}(0)\rangle^2$ , solid purple lines to  $G_{coh,\rho}^{(2)}(\tau)/\langle\hat{I}_{St}(0)\rangle^2$ , and dashed red lines to the total correlation of Stokes-shifted photons  $g_{St}^{(2)}(\tau)$  (given by the summation of the three former quantities). We simulate in (a) the molecular configuration used in Fig. 3a of the main text (all the parameters are specified in the third row of Table S1), and in (b) the molecular configuration used in Fig. 3c of the main text (all the parameters are specified in the fourth row of Table S1).

property of trace, we rewrite the numerator in Eq. (S4) as

$$\begin{aligned}
G_{St}^{(2)}(\tau)/|\xi_{St}|^4 = & p_{ee} \langle v_1 e_2 | \hat{I}_{St}(\tau) | v_1 e_2 \rangle + p_{ee} \langle e_1 v_2 | \hat{I}_{St}(\tau) | e_1 v_2 \rangle + p_{eg} \langle v_1 g_2 | \hat{I}_{St}(\tau) | v_1 g_2 \rangle \\
& + p_{ge} \langle g_1 v_2 | \hat{I}_{St}(\tau) | g_1 v_2 \rangle + p_{ev} \langle v_1 v_2 | \hat{I}_{St}(\tau) | v_1 v_2 \rangle + p_{ve} \langle v_1 v_2 | \hat{I}_{St}(\tau) | v_1 v_2 \rangle \\
& + (\langle v_1 e_2 | \hat{I}_{St}(\tau) | e_1 v_2 \rangle + \langle e_1 v_2 | \hat{I}_{St}(\tau) | v_1 e_2 \rangle) p_{ee} \\
& + \rho_{eg,ee} [\langle v_1 e_2 | \hat{I}_{St}(\tau) | v_1 g_2 \rangle + \langle e_1 v_2 | \hat{I}_{St}(\tau) | v_1 g_2 \rangle] + \rho_{ge,ee} [\langle v_1 e_2 | \hat{I}_{St}(\tau) | g_1 v_2 \rangle + \langle e_1 v_2 | \hat{I}_{St}(\tau) | g_1 v_2 \rangle] \\
& + \rho_{ee,eg} [\langle v_1 g_2 | \hat{I}_{St}(\tau) | e_1 v_2 \rangle + \langle v_1 g_2 | \hat{I}_{St}(\tau) | v_1 e_2 \rangle] + \rho_{ee,ge} [\langle g_1 v_2 | \hat{I}_{St}(\tau) | e_1 v_2 \rangle + \langle g_1 v_2 | \hat{I}_{St}(\tau) | v_1 e_2 \rangle] \\
& + (\rho_{ee,ve} + \rho_{ee,ev}) [\langle v_1 v_2 | \hat{I}_{St}(\tau) | v_1 e_2 \rangle + \langle v_1 v_2 | \hat{I}_{St}(\tau) | e_1 v_2 \rangle] \\
& + (\rho_{ve,ee} + \rho_{ev,ee}) [\langle e_1 v_2 | \hat{I}_{St}(\tau) | v_1 v_2 \rangle + \langle v_1 e_2 | \hat{I}_{St}(\tau) | v_1 v_2 \rangle] \\
& + (\rho_{eg,ev} + \rho_{eg,ve}) \langle v_1 v_2 | \hat{I}_{St}(\tau) | v_1 g_2 \rangle + (\rho_{ge,ev} + \rho_{ge,ve}) \langle v_1 v_2 | \hat{I}_{St}(\tau) | g_1 v_2 \rangle \\
& + (\rho_{ev,eg} + \rho_{ve,eg}) \langle v_1 g_2 | \hat{I}_{St}(\tau) | v_1 v_2 \rangle + (\rho_{ev,ge} + \rho_{ve,ge}) \langle g_1 v_2 | \hat{I}_{St}(\tau) | v_1 v_2 \rangle \\
& + \rho_{eg,ge} \langle g_1 v_2 | \hat{I}_{St}(\tau) | v_1 g_2 \rangle + \rho_{ge,eg} \langle v_1 g_2 | \hat{I}_{St}(\tau) | g_1 v_2 \rangle + (\rho_{ev,ve} + \rho_{ve,ev}) \langle v_1 v_2 | \hat{I}_{St}(\tau) | v_1 v_2 \rangle.
\end{aligned} \tag{S7}$$

This expression can be decomposed into three different contributions

$$G_{St}^{(2)}(\tau) = G_d^{(2)}(\tau) + G_{coh,I}^{(2)}(\tau) + G_{coh,\rho}^{(2)}(\tau). \tag{S8}$$

The first contribution is given by the six terms in the first two lines of Eq. (S7),

$$\begin{aligned}
G_d^{(2)}(\tau)/|\xi_{St}|^4 = & p_{ee} \langle v_1 e_2 | \hat{I}_{St}(\tau) | v_1 e_2 \rangle + p_{ee} \langle e_1 v_2 | \hat{I}_{St}(\tau) | e_1 v_2 \rangle + p_{eg} \langle v_1 g_2 | \hat{I}_{St}(\tau) | v_1 g_2 \rangle \\
& + p_{ge} \langle g_1 v_2 | \hat{I}_{St}(\tau) | g_1 v_2 \rangle + p_{ev} \langle v_1 v_2 | \hat{I}_{St}(\tau) | v_1 v_2 \rangle + p_{ve} \langle v_1 v_2 | \hat{I}_{St}(\tau) | v_1 v_2 \rangle,
\end{aligned} \tag{S9}$$

involving only diagonal elements of  $\hat{\rho}_{ss}$  and of  $\hat{I}_{St}(\tau)$ . The second contribution includes the terms in the third line of Eq. (S7)

$$G_{coh,I}^{(2)}(\tau)/|\xi_{St}|^4 = p_{ee} (\langle v_1 e_2 | \hat{I}_{St}(\tau) | e_1 v_2 \rangle + \langle e_1 v_2 | \hat{I}_{St}(\tau) | v_1 e_2 \rangle), \tag{S10}$$

which involves diagonal elements of the density matrix (populations) and off-diagonal elements of the operator  $\hat{I}_{St}(\tau)$ .

The rest of terms in Eq. (S7) include off-diagonal elements of the steady-state density matrix. In this way, we define

$$\begin{aligned}
G_{coh,\rho}^{(2)}(\tau)/|\xi_{St}|^4 &= \rho_{eg,ee}[\langle v_1 e_2 | \hat{I}_{St}(\tau) | v_1 g_2 \rangle + \langle e_1 v_2 | \hat{I}_{St}(\tau) | v_1 g_2 \rangle] + \rho_{ge,ee}[\langle v_1 e_2 | \hat{I}_{St}(\tau) | g_1 v_2 \rangle + \langle e_1 v_2 | \hat{I}_{St}(\tau) | g_1 v_2 \rangle] \\
&+ \rho_{ee,eg}[\langle v_1 g_2 | \hat{I}_{St}(\tau) | e_1 v_2 \rangle + \langle v_1 g_2 | \hat{I}_{St}(\tau) | v_1 e_2 \rangle] + \rho_{ee,ge}[\langle g_1 v_2 | \hat{I}_{St}(\tau) | e_1 v_2 \rangle + \langle g_1 v_2 | \hat{I}_{St}(\tau) | v_1 e_2 \rangle] \\
&+ (\rho_{ee,ve} + \rho_{ee,ev})[\langle v_1 v_2 | \hat{I}_{St}(\tau) | v_1 e_2 \rangle + \langle v_1 v_2 | \hat{I}_{St}(\tau) | e_1 v_2 \rangle] \\
&+ (\rho_{ve,ee} + \rho_{ev,ee})[\langle e_1 v_2 | \hat{I}_{St}(\tau) | v_1 v_2 \rangle + \langle v_1 e_2 | \hat{I}_{St}(\tau) | v_1 v_2 \rangle] \\
&+ (\rho_{eg,ev} + \rho_{eg,ve}) \langle v_1 v_2 | \hat{I}_{St}(\tau) | v_1 g_2 \rangle + (\rho_{ge,ev} + \rho_{ge,ve}) \langle v_1 v_2 | \hat{I}_{St}(\tau) | g_1 v_2 \rangle \\
&+ (\rho_{ev,eg} + \rho_{ve,eg}) \langle v_1 g_2 | \hat{I}_{St}(\tau) | v_1 v_2 \rangle + (\rho_{ev,ge} + \rho_{ve,ge}) \langle g_1 v_2 | \hat{I}_{St}(\tau) | v_1 v_2 \rangle \\
&+ \rho_{eg,ge} \langle g_1 v_2 | \hat{I}_{St}(\tau) | v_1 g_2 \rangle + \rho_{ge,eg} \langle v_1 g_2 | \hat{I}_{St}(\tau) | g_1 v_2 \rangle + (\rho_{ev,ve} + \rho_{ve,ev}) \langle v_1 v_2 | \hat{I}_{St}(\tau) | v_1 v_2 \rangle.
\end{aligned} \tag{S11}$$

Furthermore, we derive the analytical expressions at  $\tau = 0$  of the three contributions in which we have decomposed  $G_{St}^{(2)}(\tau)$ . With this aim, we evaluate the expression of the operator  $\hat{I}_{St}(\tau)$  in Eq. (S5) at such time delay. On the one hand, we find that all the elements  $\langle a_1 b_2 | \hat{I}_{St}(\tau) | c_1 d_2 \rangle$  in Eq. (S11) vanish at  $\tau = 0$ , which results in

$$G_{coh,\rho}^{(2)}(0) = 0. \tag{S12}$$

Notably, we have found numerically that  $G_{coh,\rho}^{(2)}(\tau)$  can become nonzero and comparable to  $G_d^{(2)}(\tau)$  at larger times, as discussed below and illustrated in Fig. S2. On the other hand, we find that  $G_d^{(2)}(0)$  and  $G_{coh,I}^{(2)}(0)$  are identical and given by

$$G_d^{(2)}(0)/|\xi_{St}|^4 = G_{coh,I}^{(2)}(0)/|\xi_{St}|^4 = 2p_{ee}. \tag{S13}$$

However, we have found numerically that  $G_{coh,I}^{(2)}(\tau)/|\xi_{St}|^4$  decays to 0 in the timescale of the vibrational lifetime, in contrast to  $G_d^{(2)}(\tau)/|\xi_{St}|^4$  that remains almost constant a larger time. Thus,  $G_{St}^{(2)}(\tau)/|\xi_{St}|^4$  is equal to  $4\rho_{ee}$  at  $\tau = 0$  and decays to  $\approx 2\rho_{ee}$  in the timescale of the vibrational lifetime. Therefore, the normalized intensity correlation  $g_{St}^{(2)}(\tau)$  also decays to half its initial value in the same timescale, which explains the narrow peak emerging at  $\tau = 0$  in those figures of the main text where  $g_{St}^{(2)}(0)$  is significantly larger than 0.

Last, to illustrate the behaviour of the different contributions in which we have decomposed  $G_{St}^{(2)}(\tau)$ , we plot in Fig. S2 the dependence on  $\tau$  of  $G_d^{(2)}(\tau)/\langle \hat{I}_{St}(0) \rangle^2$  (solid green line),  $G_{coh,I}^{(2)}(\tau)/\langle \hat{I}_{St}(0) \rangle^2$  (solid orange line),  $G_{coh,\rho}^{(2)}(\tau)/\langle \hat{I}_{St}(0) \rangle^2$  (solid purple line) and of the total correlation  $g_{St}^{(2)}(\tau)$  of Stokes shifted-photons (dashed red line). In particular, in Fig. S2a we fix the molecular configuration used in the simulations in Fig. 3a of the main text (i.e., the emitters are moderately coupled and driven by a laser tuned to the two-photon resonance  $\omega_L = \omega_0$ , the rest of parameters are detailed in the third row of Table S1). We find that the two contributions to the numerator of the correlation of Stokes-shifted photons that involve quantum coherences vanish at large delay times, i.e.,  $G_{coh,I}^{(2)}(\tau \rightarrow \infty) = G_{coh,\rho}^{(2)}(\tau \rightarrow \infty) = 0$ . Additionally,  $G_{coh,I}^{(2)}(\tau)$  is only non-zero at very short delay times, being responsible of the extremely narrow peak of the total correlation of Stokes-shifted photons  $g_{St}^{(2)}(\tau)$  around  $\tau = 0$ , as commented above. On the other hand,  $G_{coh,\rho}^{(2)}(\tau)$  becomes important in the time-scale of the lifetime of the electronic excited states and can take either positive and negative values. A similar behaviour of these quantities is observed in Fig. S2b, where we fix the molecular configuration used in Fig. 3c of the main text, corresponding to two molecules separated by a much larger distance  $r_{12} = 400$  nm (the rest of parameters are specified in the fourth row of Table S1).

## V. ALTERNATIVE MASTER EQUATION

In this section we present an alternative Markovian Master Equation to that presented in Eq. (2) of the main text and show that both of them give almost identical results. This alternative Markovian Master Equation is given as

$$\frac{d}{dt} \hat{\rho} = -\frac{i}{\hbar} [\hat{H}, \hat{\rho}] + \sum_{j=1}^2 \left( \frac{\gamma_v}{2} \mathcal{D}[[g_j] \langle v_j \rangle] + \frac{\gamma_j}{2} \mathcal{D}[\hat{\sigma}_j] + \sum_{k \neq j}^2 \frac{\gamma_{jk}}{2} \mathcal{D}[\hat{\sigma}_j, \hat{\sigma}_k] \right), \tag{S14}$$

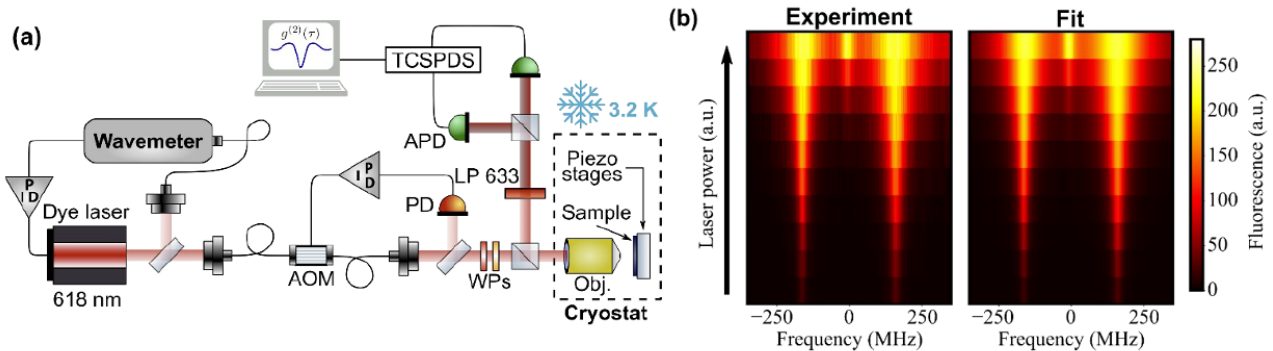


FIG. S3. (a) Schematic representation of the experimental setup used to measure the correlation of Stokes-shifted photons  $g_{St}^{(2)}(\tau)$ . The intensity of the laser is stabilized using a photodiode (PD) in combination with an acousto-optic modulator (AOM). A wavemeter is employed to lock the laser frequency close to the molecular transition. The laser beam is tightly focused on two coupled emitters using a high-numerical-aperture microscope objective (NA 0.95), which also collects the emitted photons. A long-pass filter selectively transmits red-shifted photons above 633 nm, ensuring spectral isolation. The filtered photons are directed to the detection system, which comprises two avalanche photodiodes (APDs) connected to a time-correlated single-photon detection system (TCSPDS). (b) Experimental and fitted excitation spectra as a function of laser power, ranging from 2 nW to 1024 nW. The experimental data points are compared to theoretical fits to extract the parameters of the pairs (coupling constant  $V$ , detuning  $\delta$  between the two emitters and crossed decay rate  $\gamma_{12}$ ).

where  $\hat{H}$  is the total Hamiltonian presented in the main text. Here, the total decay rate  $\gamma_0$  is directly assigned to the dissipator related to the decay from  $|e_j\rangle$  to  $|g_j\rangle$  (the Zero-Phonon Line). This approach is different to the one followed in Eq. (2) of the main text, where the dissipation from the excited state  $|e_j\rangle$  is decomposed into the contribution from the radiative decay to  $|g_j\rangle$  (with rate  $\alpha\gamma_0$ ) and from the radiative decay to  $|v_j\rangle$  [with rate  $(1-\alpha)\gamma_0$ ].

We have compared the correlation of Stokes-shifted photons  $g_{St,alt}^{(2)}(\tau)$  obtained using this alternative Markovian Master equation with the correlation  $g_{St}^{(2)}(\tau)$  obtained using Eq. (2) of the main text for all simulations in Fig. 2 and Fig. 3 in the main text. The maximum deviation  $|g_{St,alt}^{(2)}(\tau) - g_{St}^{(2)}(\tau)|/g_{St}^{(2)}(\tau)$  is obtained at  $\tau = 0$  in Fig. 2c (two strongly interacting molecules driven by a laser tuned to the two-photon resonance) and its value is  $\approx 7 \cdot 10^{-4}$ .

## VI. EXPERIMENTAL SETUP

In this section we describe the experimental setup that we have used to measure the correlation of Stokes-shifted photons emitted from pairs of DBATT molecules. This setup is illustrated in Fig. S3a, where a continuous-wave (CW) laser (ring dye laser, Coherent 699) is employed to excite pairs of dibenzanthanthrene (DBATT) molecules, which are randomly embedded in a thin naphthalene film with a thickness of less than a few micrometers. To ensure stability, the laser frequency is digitally locked to a wavemeter (High Finesse WS7) with a relative precision of 1 MHz, preventing long-term drifts. The laser frequency can be manually adjusted by changing the lock point, allowing precise detuning with respect to the desired molecular transition. Additionally, the laser power is stabilized in a closed-loop system with a bandwidth of few kHz, using a fiber-coupled acousto-optic modulator (AOM). The AOM's transmission is controlled by adjusting its driving electrical power, ensuring consistent laser output for the experiments.

The sample is cooled to 3.2 K using a closed-cycle pulsed tube cryostat, where it is mounted on a piezo stage for precise positioning. The laser is focused using a high numerical aperture (NA = 0.95) microscope objective, which is also employed to collect emitted fluorescence photons. A long-pass filter (LP 633) is utilized to isolate Stokes-shifted photons while removing the ZPL and laser photons. The collected photons are directed to two avalanche photodiodes (SPCM-AQRH-15-FC, Excelitas) in a Start-Stop configuration to measure the intensity correlation. The time-histogram of photon detection statistics is reconstructed using a commercial Time-Correlated Single Photon Detection System (TCSPDS, TimeHarp 260), with a binning time width of 308 ps. Due to the time resolution limitations of the avalanche photodiodes (APDs), which exhibit a jitter of approximately 400 ps (FWHM), only frequencies below 1 GHz can be reliably resolved in our measurements. As a result, our experimental setup is unable to capture the dynamics associated with the vibrational states, whose lifetimes are on the order of 10 ps. This

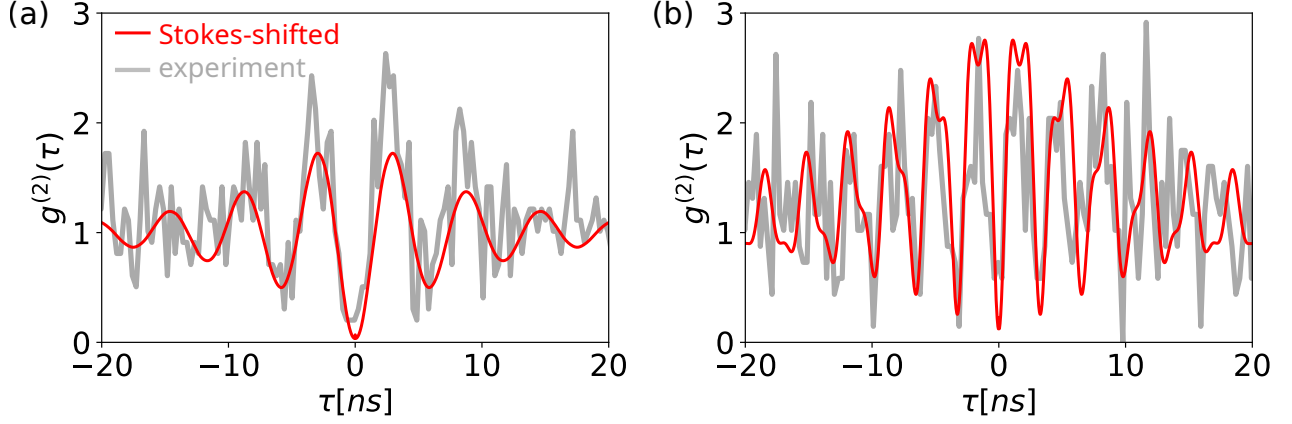


FIG. S4. Correlation of Stokes-shifted photons emitted from a pair of DBATT molecules in a H-aggregate configuration, with  $V = 9.19\gamma_0$  and  $\gamma_{12} = 0.3\gamma_0$ . Solid red lines correspond to the numerical result of the model that we propose in the main text, and solid grey lines correspond to experimental measurements. The rest of molecular and laser parameters are specified in Table S2.

limitation justifies the absence of the extremely narrow peak at  $\tau = 0$  obtained in the simulated intensity correlation in Fig. 2c and Fig. 3 of the main text.

Moreover, the molecular detuning  $\delta$ , the coherent dipole-dipole coupling  $V$  and the crossed decay rate  $\gamma_{12}$  of each pair are extracted through a two-dimensional fit of a series of excitation spectra measured at different laser intensities [2]. In Fig. S4b, we plot the Stokes-shifted excitation spectra for the molecular pair presented in Figs. 3a and 3c of the main text. In these spectra, the transitions to the superradiant and subradiant states are clearly identified, as well as the central two-photon transition that becomes prominent when the laser power increases. Numerically, the excitation spectra is proportional to  $\langle \hat{I}_{St}(0) \rangle$  [see Eq. (S6)]. The fit of  $\langle \hat{I}_{St}(0) \rangle$  (which is in excellent agreement with the experimental excitation spectra) yields  $\delta \approx 5\gamma_0$ ,  $V \approx 2.98\gamma_0$  and  $\gamma_{12} \approx 0.29\gamma_0$ , with  $\gamma_0 = 21.5$  MHz. Additionally, the transition dipole moments are found to be nearly parallel, forming a H-aggregate configuration (see Section I of this Supplementary Material). We follow an identical procedure to fit the parameters of the molecular pair used in Fig. S4 and in Fig. 2 (which are specified in the second row of Table S1), with experimental data reported in Ref. [2].

## VII. FURTHER EXPERIMENTAL MEASUREMENTS

With the purpose of further verifying the accuracy of the model that we propose in the main text, we have performed additional experimental measurements of the correlation of Stokes-shifted photons emitted from a different pair of interacting DBATT molecules. This pair forms a molecular H-aggregate, with  $V = 9.19\gamma_0$  and dissipative coupling  $\gamma_{12} \approx 0.3\gamma_0$ , which is extracted by fitting the experimental excitation spectrum (as discussed in section V of this Supplementary Material). In the experiment, we apply different voltages to the naphthalene crystal in which the molecules are immersed, which enables to modify the molecular detuning  $\delta$  [2].

First, in Fig. S4a we show the experimental measurements (grey line) obtained when the laser is slightly detuned from the superradiant state, similarly to Fig. 2a of the main text. However, in contrast to Fig. 2a of the main text, here the molecular detuning  $\delta$  is considerably larger than the dipole-dipole coupling  $V$  and, additionally, the molecular pair is driven by a more intense laser. We find that the intensity correlation resembles that in Fig. 2a, but exhibiting faster oscillations with the time delay. The experimental measurement is well reproduced by the simulated intensity

Figure	$\mu_j/ \mu_j $	$\gamma_0/(2\pi)$ [MHz]	$\alpha$	$V/\gamma_0$	$\gamma_{ij}/\gamma_0$	$\delta/\gamma_0$	$\Lambda/\gamma_0$	$\omega_L$	$ \Omega_j /\gamma_0$	$\mathbf{k}_L/ \mathbf{k}_L $	$\phi_{St}$	$\hbar\omega_v$ [meV]	$1/\gamma_v$ [ps]
Fig. S4a	$\hat{x}$	21.5	0.3	-17	0.3	41.44	22.67	$\omega_0 + 21.95\gamma_0$	3.15	$\hat{y}$	0	31.86	10
Fig. S4b	$\hat{x}$	21.5	0.3	2.98	0.29	36.63	20.49	$\omega_0 - 6.98\gamma_0$	1.5	$\hat{y}$	0	31.86	10

TABLE S2. Molecular and laser parameters used in the simulations in Fig. S4a (second row) and in Fig. S4b (third row).



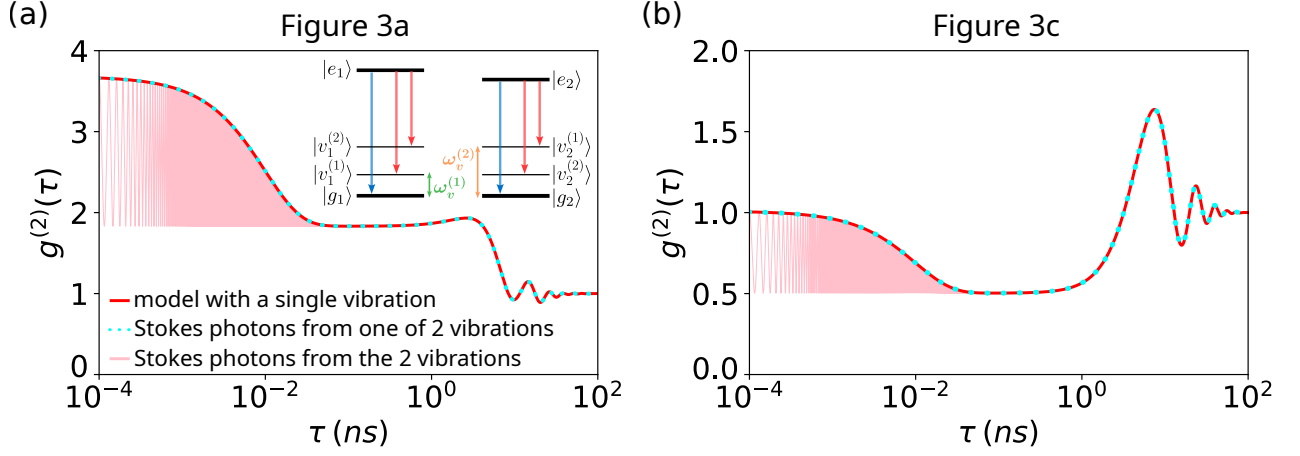


FIG. S5. Comparison of the simulated correlation of Stokes-shifted photons emitted from two DBATT molecules when different number of 1-phonon states are considered. Red lines represent simulations obtained with the model presented in the main text, where a single 1-phonon state is considered in each emitter. Additionally, we perform simulations using the Master Equation in Eq. (S16), where two 1-phonon states  $|v_j^{(1)}\rangle$  (with frequency  $\omega_v^{(1)}$  corresponding to the vibrational mode  $257\text{ cm}^{-1}$  of the DBATT molecules) and  $|v_j^{(2)}\rangle$  (with frequency  $\omega_v^{(2)}$  corresponding to the vibrational mode  $1331\text{ cm}^{-1}$  of the DBATT molecules). In the inset in (a) we depict the energy levels within this latter model, with the red arrows corresponding to the different Stokes-shifted transitions and the blue arrows to the ZPL transitions. Importantly, we use this latter that includes additional 1-phonon states to simulate the correlation of Stokes-shifted photons in two different scenarios: (i) considering the Stokes-shifted photons emitted due to the assistance of the two vibrational levels of each emitter (solid pink lines), and (ii) considering only the Stokes-shifted photons emitted due to the assistance of the vibrational mode of frequency  $\omega_v^{(1)}$  (dotted cyan lines), which experimentally correspond to filter only the Stokes-shifted photons from this vibrational mode. In (a) we fix the molecular configuration used in Fig. 3a of the main text, where two interacting molecules are driven by a laser tuned to the two-photon resonance  $\omega_L = \omega_0$  (all the parameters are detailed in the third row of Table S1), and in (b) we simulate the molecular configuration used in Fig. 3c of the main text, where the two emitters are at very far distances and again  $\omega_L = \omega_0$  (all the parameters are specified in the fourth row of Table S1).

correlation (red line), which is obtained using the complete model presented in the main text and considering again normal incidence and detection of light (the rest of parameters are specified in the second row of Table S2).

Moreover, in the experiment shown in Fig. S4b the molecular detuning is also large compared to the dipole-dipole coupling strength but, in contrast to Fig. S4a, the laser frequency is now moderately detuned from the two-photon resonance. In this case, the experimental intensity correlation exhibits even faster oscillations with the time delay, which are well reproduced by our simulations (all parameters used in the simulation are specified in the third row of Table S2).

### VIII. IMPACT OF A LARGER NUMBER OF VIBRATIONAL MODES

In this section we analyze the impact of including additional 1-phonon states in the Hamiltonian and the Master Equation, corresponding to other vibrational modes in the electronic ground state. More specifically, we consider that each emitter supports two vibrational modes of frequencies  $\omega_v^{(1)}$  and  $\omega_v^{(2)}$ , with corresponding 1-phonon states denoted as  $|v_j^{(n)}\rangle$  (here,  $j = 1, 2$  labels each emitter). We represent an scheme of the energy levels of the uncoupled emitters in the inset of Fig. S5a. The Hamiltonian of the system can thus be written as

$$\hat{H} = \hbar \sum_{j=1}^2 \left[ \frac{\Delta_j}{2} (|e_j\rangle \langle e_j| - |g_j\rangle \langle g_j|) + \sum_n \frac{2\omega_v^{(n)} - \Delta_j}{2} |v_j^{(n)}\rangle \langle v_j^{(n)}| \right] + \hat{H}_I + \hat{H}_P, \quad (\text{S15})$$

where the interaction and pumping Hamiltonians are again given as  $\hat{H}_I = \hbar V (\hat{\sigma}_1^\dagger \hat{\sigma}_2 + \hat{\sigma}_1 \hat{\sigma}_2^\dagger)$  and  $\hat{H}_P = -\frac{\hbar}{2} \sum_{j=1}^2 (\Omega_j \hat{\sigma}_j^\dagger + \Omega_j^* \hat{\sigma}_j)$ , respectively. The Markovian Master equation including the dissipative processes and governing the dynamics

of the system is given as

$$\frac{d}{dt}\hat{\rho} = -\frac{i}{\hbar}[\hat{H}, \hat{\rho}] + \sum_{j=1}^2 \left( \frac{\alpha\gamma_j}{2} \mathcal{D}[\hat{\sigma}_j] + \sum_{k \neq j} \frac{\gamma_{jk}}{2} \mathcal{D}[\hat{\sigma}_j, \hat{\sigma}_k] + \sum_n \left[ \frac{(1-\alpha)\gamma_j}{4} \mathcal{D}[|v_j^{(n)}\rangle \langle e_j|] + \frac{\gamma_v}{2} \mathcal{D}[|g_j\rangle \langle v_j^{(n)}|] \right] \right) \rho, \quad (\text{S16})$$

where we have assumed that the decay rate from  $|e_j\rangle$  to  $|v_j^{(1)}\rangle$  is  $(1-\alpha)\gamma_j/2$  and identical to the decay rate from  $|e_j\rangle$  to  $|v_j^{(2)}\rangle$ . These latter dissipation processes are represented by red arrows in the inset in Fig. S5a, whereas the dissipation in the Zero-Phonon Line (having decay rate  $\alpha\gamma_j$ ) is represented with blue arrows.

Next we simulate again the correlation of Stokes-shifted photons emitted from two DBATT molecules at cryogenic temperatures. We use  $\hbar\omega_v^{(1)} = 31.86$  meV and  $\hbar\omega_v^{(2)} = 165.02$  meV, which correspond to the the  $257$   $\text{cm}^{-1}$  and  $1331$   $\text{cm}^{-1}$  vibrational modes, respectively, of the DBATT molecules [4]. In Fig. S5a we fix the same molecular configuration than in Fig. 3a of the main text, in which two interacting molecules are driven by a laser tuned to the two-photon resonance  $\omega_L = \omega_0$  (the rest of parameters are specified in the third row of Table S1). On the one hand, we use  $\hat{E}_{\text{St}}^{(+)}(t)/\xi_{\text{St}} = \sum_n |v_1^{(n)}\rangle \langle e_1| (t) + |v_2^{(n)}\rangle \langle e_2| (t)$  to calculate the intensity correlation of Stokes-shifted photons emitted from the two molecules due to the assistance of the two-vibrational modes. The resulting intensity correlation (solid pink line) shows the same behaviour than the simulation obtained in the main text including a single vibrational mode in the Master Equation (red solid line) at delay times larger than the lifetime of the vibrations ( $\tau \gg 1/\gamma_v$ ). However, in the timescale of the vibrations lifetime we find that the decay of the intensity correlation to half its value at  $\tau = 0$  (which is due to the loss of coherence, as discussed in the main text and in Section III of this Supplemental Material) is accompanied by fast oscillations of frequency  $\omega_v^{(2)} - \omega_v^{(1)}$ . Additionally, we calculate the intensity correlation using  $\hat{E}_{\text{St}}^{(+)}(t)/\xi_{\text{St}} = |v_1^{(1)}\rangle \langle e_1| (t) + |v_2^{(1)}\rangle \langle e_2| (t)$  (cyan dotted line), which represents the correlation of Stokes-shifted photons that are due only to the assistance of the vibrational mode  $257$   $\text{cm}^{-1}$ . We find that this latter simulated intensity correlation is identical to the one obtained in the main text using a Master Markovian equation that includes a single vibrational mode.

---

\* adrianjuand1996@gmail.com

† aizpurua@ehu.eus

- [1] A. Stokes and A. Nazir, “A master equation for strongly interacting dipoles,” *New Journal of Physics* **20**, 043022 (2018).
- [2] J.B. Trebbia, Q. Deplano, P. Tamarat, and B. Lounis, “Tailoring the superradiant and subradiant nature of two coherently coupled quantum emitters,” *Nature Communications* **13**, 1–9 (2022).
- [3] A. Juan-Delgado, R. Esteban, Á. Nodar, J.-B. Trebbia, B. Lounis, and J. Aizpurua, “Tailoring the statistics of light emitted from two interacting quantum emitters,” *Physical Review Research* **6**, 023207 (2024).
- [4] F. Jelezko, B. Lounis, and M. Orrit, “Pump–probe spectroscopy and photophysical properties of single di-benzanthanthrene molecules in a naphthalene crystal,” *The Journal of chemical physics* **107**, 1692–1702 (1997).